International Journal of Multiphase Flow 36 (2010) 558–569

Contents lists available at ScienceDirect

International Journal of Multiphase Flow

journal homepage: www.elsevier.com/locate/ijmulflow

A diffuse-interface approach to two-phase isothermal flow of a Van der Waals fluid near the critical point

A. Pecenko *, J.G.M. Kuerten, C.W.M. van der Geld

Eindhoven University of Technology, Dept. of Mechanical Engineering, Den Dolech 2, P.O. Box 513, 5600 MB, Eindhoven, The Netherlands

ARTICLE INFO

Article history:
Received 23 October 2009
Received in revised form 15 January 2010
Accepted 15 March 2010
Available online 23 March 2010

Keywords:
Diffuse interface
Critical point
Korteweg tensor
Van der Waals

ABSTRACT

A novel numerical method for simulations of isothermal, compressible two-phase flows of one fluid component near the critical point is presented on the basis of a diffuse-interface model and a Van der Waals equation of state. Because of the non-convexity of the latter, the nature of the set of governing equations is mixed hyperbolic–elliptic. This prevents the application of standard numerical methods for compressible flow. Moreover, the Korteweg capillary stress tensor, characteristic for the diffuse-interface approach, introduces third-order spatial derivatives of mass density in the Navier–Stokes equation, resulting in a dispersive behavior of the solution. Our computational method relies on a transformation of the conserved variables, which controls dispersion, stabilizes the numerical simulation and enables the use of coarser grids. A one-dimensional simulation shows that this method provides better stability and accuracy than without transformation of variables. Two- and three-dimensional simulations for isothermal liquid–vapor flows, in particular the retraction of a liquid non-spherical drop in vapor and the binary droplet collision in vapor, show the applicability of the method. The surface tension calculated from the numerical results is in good agreement with its theoretical value if the computational grid is sufficiently fine.

1. Introduction

Over the past decades, a great deal of effort has been addressed towards mathematically consistent descriptions of flows in the presence of *interfaces*, that is surfaces of separation between different thermodynamic phases of a single compound or between different fluids. Such multiphase/multifluid flows occur in numerous industrial applications and geophysical phenomena. From a physical point of view, interfaces are never sharp, but they can be regarded as thin layers of fluid where properties such as mass density, pressure and viscosity change continuously between the values of the bulk fluid regions. Methods that treat the interfaces as finite portions of the fluid domain are called *diffuse-interface* methods.

Although a diffuse-interface method seems the most natural approach, computational methods that make use of the assumption of zero interface thickness are at present more popular in the literature. They are called *sharp-interface* methods. The main reason for their widespread use is probably the small numerical grid spacing required for the resolution of the interface in a diffuse-interface method. In the case of one-component multiphase systems, the interface thickness depends solely on temperature and becomes infinite at the critical point where only the gaseous phase of a substance exists. At temperatures that are not in the vicinity of the critical value, the thickness of a liquid–vapor interface typically attains the order of a few molecule diameters. Consequently, a direct numerical simulation aiming to capture both the scales of the size of the interface thickness and those of the order of a typical drop or bubble diameter is unfeasible.

In a diffuse-interface method a unique set of governing equations describes the complete two-phase domain and no interface tracking or reconstruction, necessary in sharp-interface methods, is required. From this point of view, diffuse-interface methods present the same advantages over the tracking methods as the Level-Set method does. In the latter, however, determining the actual position of the interface requires the solution of an additional evolution equation for a level function. Moreover, the explicit form of such equation depends on the particular problem considered (see for example Mulder et al., 1992).

Here, an extra contribution to the stress tensor, which accounts for the capillary stresses at the interface, is added to the momentum conservation equation, instead. The usual choice for this tensor is the second-order frame-invariant Korteweg tensor, which depends on the mass density and its spatial derivatives (Korteweg, 1901), and represents long-ranged molecular interactions (Bongiorno et al., 1976). Continuum-type formulations of flows with fluid

* Corresponding author. Tel.: +31 402472573.
E-mail addresses: a.pecenko@tue.nl (A. Pecenko), j.g.m.kuerten@tue.nl (J.G.M. Kuerten), c.w.m.v.d.geld@tue.nl (C.W.M. van der Geld).

0301-9322/$ - see front matter © 2010 Elsevier Ltd. All rights reserved.
doi:10.1016/j.ijmultiphaseflow.2010.03.005

surfaces of separation that adopt Korteweg's stress tensor have also been used for multifluid problems, such as displacements of a fluid into another miscible and more viscous fluid in porous environment (Chen et al., 2001) or in capillary tubes (Chen and Meiburg, 2002). In such cases, Korteweg stresses originate from concentration gradients.

For a multiphase flow of the same fluid component, including Korteweg's tensor in the momentum equation makes the mass density continuous everywhere in the domain. Moreover, there is no need to introduce singularities in order to include surface tension in the equations. This is an advantage over other one-fluid formulations since topological changes of the interface in dynamical conditions, as well as integral properties such as surface tension, are accounted for in the solution. Hence, no special treatment for complex, time-dependent interface topologies is required.

Another advantage of the diffuse-interface method with Korteweg's stress tensor is that the thickness of an interface is not artificially increased, as in some sharp-interface methods like the Volume-of-Fluid method. Moreover, phase transitions are accounted for in the governing equations in a physical way.

Recently, it has been shown (Lamorgese and Mauri, 2009) that it is possible to apply the diffuse-interface approach to two-phase flows and capture the finite interfacial zones with sufficient accuracy on uniform grids that do not require an excessively large number of nodes. For this application to be successful two conditions have to be met. First, the two-phase system should be close to the critical temperature and second, the characteristic length of the computational domain should be sufficiently small so that only a few drops and/or bubbles can be present. In some applications of the diffuse-interface method with Korteweg's formulation of the capillary tensor (Jamet et al., 2001) these conditions are relaxed by artificially increasing the interface thickness. Although the use of an artificial thickness enables larger computational domains and wider ranges of temperature, the thermodynamic behavior of the fluid has to be modified, which leads to modifications in macroscopic properties as well (Jamet et al., 2001; Verschueren et al., 2001).

Numerical solution methods for the governing equations of the diffuse-interface method with Korteweg's stress tensor for a liquid–vapor flow have to cope with two additional problems, compared to single-phase flow. First, the Korteweg tensor leads to dispersive behavior of the solution, since it contains a second-order spatial derivative of the mass density. Second, an equation of state, which captures the behavior of both liquid and vapor phases, such as the Van der Waals equation, always has a non-convex part. This leads to mixed hyperbolic–elliptic nature of the set of governing equations, instead of the purely hyperbolic nature for an ideal gas, and prevents the application of standard numerical methods for compressible flow simulation.

In this paper we will develop a numerical method suitable to cope with these two problems and apply it to several standard cases for two-phase flow in two and three spatial dimensions. The advantage of the present method over other methods used in the literature is that it is applied after a transformation of the dependent variables, which removes the major terms responsible for the dispersive nature of the set of equations. The transformation of variables is based on the work developed in Cockburn and Gau (1996) for one-dimensional, inviscid phase transitions in solids. The transformation is possible if the Reynolds number based on the interface thickness is not too large. We will show that the transformation stabilizes the numerical method significantly and hence allows the use of coarser grids.

We focus on isothermal liquid–vapor flows near the critical temperature, for which the choice of the Van der Waals equation of state is the most natural. In a diffuse-interface method, viscosity and capillarity coefficient should be continuous functions of mass density. The numerical results will be validated by comparing the surface tension found from the radius of a liquid drop in steady state and the pressure drop over the interface with its theoretical value at thermodynamic equilibrium (Cahn and Hilliard, 1958; Cahn, 1959).

The paper is structured as follows. In Section 2 we briefly recall the derivation of the Korteweg tensor when the capillarity coefficient is a general function of mass density, and we describe the set of governing equations for an isothermal two-phase flow of a pure substance. Also, the consequences of a non-monotonic equation of state are briefly discussed and an energy equation is derived. In Section 3 the transformation of variables is introduced. Section 4 presents the numerical method and a one-dimensional simulation that demonstrates the stability of the method. In Section 5 we discuss the results of a two- and three-dimensional simulation of the retraction of a liquid drop in vapor to its equilibrium shape. For this problem the value of the surface tension in steady state is compared with its theoretical value, a grid refinement study is performed and the advantage of the transformation of variables is demonstrated by a comparison of results with and without transformation. Section 6 shows the results of two simulations of the two-dimensional binary droplet collision with subsequent coalescence, at different Weber number. Finally, in Section 7 some conclusions are drawn.

2. Governing equations

In this section, we outline the derivation of the Korteweg tensor that we adopt and we present the system of governing equations. A suitable approach for the derivation of the Korteweg tensor for two-phase flow of a pure substance, in which the mass density exhibits large variations in space, is calculus of variations. The basis of the theory is the second law of thermodynamics, which states that the extrema of the free energy correspond to equilibrium. We consider a closed volume of fluid V with total mass $\mathscr{M}$. Thus, the equilibrium condition of a single-component two-phase fluid can be found by minimizing the total Helmholtz free energy of the system

$$\mathscr{F}_{tot} = \mathscr{F}_b + \mathscr{F}_s, \tag{1}$$

where $\mathscr{F}_b$ refers to the two bulk phases, while the term $\mathscr{F}_s$ accounts for the interfacial contribution. In Cahn and Hilliard (1958) it is shown that the free energy density of an isotropic medium can be expanded as a Taylor series of even powers of the mass density gradient norm. By neglecting higher order terms and integrating over a given volume V of fluid, (1) can be written in the so-called Landau–Ginzburg form

$$\mathscr{F}_{tot} = \int_V \rho f(\rho)\, dV \tag{2}$$

$$= \int_V \left[\rho f^0(\rho) + \frac{1}{2}K(\rho)|\nabla\rho|^2\right] dV, \tag{3}$$

where $\rho f(\rho)$ is the total free energy density, $\rho f^0(\rho)$ represents the free energy density of the bulk phases and $\frac{1}{2}K(\rho)|\nabla\rho|^2$ is the lowest non-zero term in the expansion, which is due to the presence of interfaces. Here, we follow Cahn (1959) in making the assumption that the coefficient K, also called *gradient energy coefficient*, is independent of the mass density gradient. However, we assume that K is a function of mass density, which is the most general assumption in the isothermal case we consider. For the case of constant K, a derivation of (3) can be found in Van der Waals (1894).

The thermodynamic equilibrium of a fixed volume of liquid and vapor of a single substance corresponds to a minimum of $\mathscr{F}_{tot}$. An Euler–Lagrange equation can be derived for the functional $\mathscr{L} = I - \lambda\rho$, where I is the integrand in (3), and λ, the Lagrangian

multiplier needed to conserve mass $\mathscr{M}$, can be identified with the chemical potential (Cahn, 1959; Pismen, 2001).

In Anderson et al. (1998), the variational procedure is elucidated for the case of constant K, which leads to a special form of the more general capillary stress tensor $\mathbf{T}$. If a gradient energy coefficient depending on mass density $K(\rho)$ is chosen, the minimization of $\mathscr{F}_{tot}$ with the mass conservation constraint leads to the following expression for the Korteweg tensor (Papatzacos, 2000)

$$\mathbf{T} = \left\{ -\rho^2 f_\rho^0 + \rho K(\rho) \triangle \rho + \frac{1}{2}(\rho K(\rho))_\rho |\nabla \rho|^2 \right\} \mathbf{I} - K(\rho) \nabla \rho \otimes \nabla \rho, \tag{4}$$

where $\rho^2 f_\rho^0$ can be identified with the thermodynamic pressure p, $\triangle\rho$ is the Laplacian of ρ and $\mathbf{I}$ the identity tensor. The subscript ρ denotes derivative with respect to mass density. In this paper, we will use (4) as capillary stress tensor. This form of the Korteweg tensor is a special case of the one obtained in Korteweg (1901) from purely mechanical considerations, which reads in its original formulation (Aifantis and Serrin, 1983b)

$$\mathbf{T} = \{ -p + \alpha \triangle \rho + \beta |\nabla \rho|^2 \} \mathbf{I} + \delta \nabla \rho \otimes \nabla \rho + \gamma (\nabla \otimes \nabla) \rho,$$

where α, β, γ and δ are functions of temperature and mass density that depend on the substance.

Typically, in the literature on two-phase flows of a pure substance, the assumption $\gamma = 0$ is made and the Korteweg tensor can be simplified to (Dunn and Serrin, 1985)

$$\mathbf{T} = \left\{ -p + \rho c \triangle \rho + \frac{1}{2}(\rho c)_\rho |\nabla \rho|^2 \right\} \mathbf{I} - c \nabla \rho \otimes \nabla \rho, \tag{5}$$

where c plays the role of a macroscopic capillarity coefficient, directly related to the surface tension, and is a function of temperature and mass density but not of the mass density gradient. By identifying the capillarity coefficient c with the gradient energy coefficient $K(\rho)$ in (3), the equivalence of (4) and (5) can be seen.

The governing equations of two-phase flow in non-equilibrium conditions are now obtained by addition of the divergence of the capillary stress tensor to the right-hand side of the Navier–Stokes equation of momentum conservation, which then reads in conservative form

$$(\rho \mathbf{u})_t + \nabla \cdot (\rho \mathbf{u}\mathbf{u}) = \nabla \cdot (\mathbf{d} + \mathbf{T}), \tag{6}$$

where the subscript t denotes time derivative, $\mathbf{u}$ is the velocity vector, and $\mathbf{d}$ denotes the viscous stress tensor with the Newtonian linear stress–strain relation

$$\mathbf{d}_{ij} = \mu(\rho) \left(\frac{\partial u_i}{\partial x_j} + \frac{\partial u_j}{\partial x_i} \right) + \eta(\rho)(\nabla \cdot \mathbf{u}) \delta_{ij},$$

where δ_{ij} is the Kronecker tensor and η is the second viscosity coefficient. In the isothermal case, where the thermodynamic pressure p is a known function of mass density, a closed system of governing equations appears if the Navier–Stokes equation is supplemented with the continuity equation for the liquid–vapor system

$$\rho_t + \nabla \cdot (\rho \mathbf{u}) = 0. \tag{7}$$

As remarked in the introduction, the Van der Waals equation of state is an appropriate choice for liquid–vapor flows near the critical temperature. Hence, at a given temperature we will use as equation of state

$$p(\rho, T) = \frac{RT}{M - b\rho} \rho - \frac{a}{M^2} \rho^2, \tag{8}$$

where R is the universal gas constant, T the prescribed absolute temperature, M the molar mass, and a and b are two constant coefficients empirically determined for the particular substance. Although this equation represents the isothermal behavior of a fluid below the condensation point and above the saturation point, each isotherm contains an unphysical region of negative compressibility $dp/d\rho < 0$. This region is highly sensitive to small perturbations, since for any value of density between the two points of infinite compressibility $dp/d\rho = 0$ the system evolves towards phase segregation (Fig. 1).

Van der Waals (1894) developed a mean-field theory of capillarity where a constant value for the gradient-energy coefficient K is assumed. Nevertheless, he recognized the possibility that K depends on the local thermodynamic state (ρ, T). In more recent works, like Bongiorno et al. (1976), this issue has been investigated in the context of a molecular theory of the interface. Here we will make a particular choice for the functional dependence of K on ρ, as shown in Section 3.

2.1. Energy equation

Dunn and Serrin (1985) describe the incompatibility of Korteweg's original formulation of the tensor $\mathbf{T}$ with the entropy condition in the classical form of the Clausius–Duhem inequality, unless the total energy balance equation is modified by postulating the existence of an unconventional, additional rate of supply of mechanical energy, which the authors call "interstitial working". When $\mathbf{T}$ has the formulation as in (4), the related extra rate of working reads $K(\rho)\frac{D\rho}{Dt}\nabla\rho$.

The purpose of this section is to derive an equation for the evolution of the total energy for the case of a compressible two-phase flow that is assumed to be isothermal. Through this derivation we will show that the rate of working $K(\rho)\frac{D\rho}{Dt}\nabla\rho$ allows to extend the isothermal approximation for compressible flow to the two-phase case. It is useful to recall that a compressible, viscous, single-phase flow in a fixed volume can only be approximately isothermal. Unlike the incompressible case, where kinetic energy strictly decreases in time provided that its flux through the domain boundaries is equal to zero, compressible flow is affected by the reversible conversion of kinetic into internal energy.

Compared to single-phase isothermal flow, the two-phase situation also involves another form of energy besides the kinetic energy, which is due to the presence of interfaces. The total energy density of the system therefore reads

$$\rho e = \frac{1}{2}\rho |\mathbf{u}|^2 + \frac{1}{2} K(\rho) |\nabla \rho|^2, \tag{9}$$

where the last term on the right-hand side is the *interfacial energy* density. This is the expression of total energy density for which we intend to derive an evolution equation.

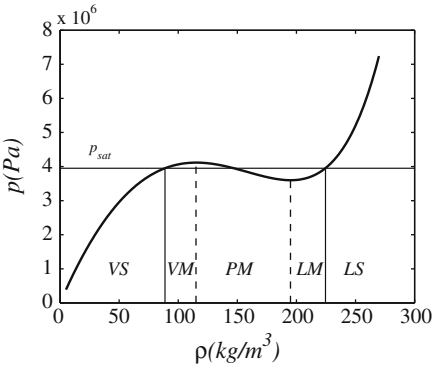

Fig. 1. A Van der Waals isotherm below the critical point in the (p, ρ) plane. The horizontal solid line represents the saturation pressure p_{sat} at the assigned temperature. The vertical lines mark the different regions of the solution domain according to the equation of state. VS = vapor stable, VM = vapor metastable, PM = phase mixture, LM = liquid metastable, LS = liquid stable. The unstable region of phase separation corresponds to the phase mixture (PM).

Differentiation of both sides of (9) with respect to time and substitution of the continuity and momentum equations yields after some calculus:

$$\frac{\partial(\rho e)}{\partial t}+\nabla\cdot(\rho e\mathbf{u})=\nabla\cdot((\mathbf{d}+\mathbf{T})\cdot\mathbf{u})-\nabla\cdot\left(K(\rho)\frac{D\rho}{Dt}\nabla\rho\right)-\Phi+p\nabla\cdot\mathbf{u}. \tag{10}$$

The second term on the left-hand side is the convective transport. The first term on the right-hand side describes the transport of total energy by viscous and interfacial forces and pressure. The second term on the right-hand side is, as anticipated, the interstitial working and is also present if the assumption of isothermal flow is not made.

In contrast with these three terms, the last two terms on the right-hand side convert energy. The third term on the right-hand side, Φ, is the energy dissipation caused by viscosity, and is given by

$$\Phi=2\mu(\rho)[u_x^2+v_y^2+w_z^2]+\eta(\rho)(\nabla\cdot\mathbf{u})^2+\mu(\rho)[(u_y+v_x)^2+(u_z+w_x)^2+(v_z+w_y)^2],$$

where u, v and w are the Cartesian components of velocity and x, y and z are the Cartesian coordinates. The energy dissipation is strictly positive if

$$\mu(\rho)>0, \tag{11}$$

$$\eta(\rho)\geqslant-\frac{2}{3}\mu(\rho). \tag{12}$$

When these conditions are satisfied, the total energy of the isothermal two-phase system strictly decreases by viscosity and is conserved by the capillary forces. The last term on the right-hand side of (10), also present if the flow is single-phase, is the reversible part of the energy conversion, identically zero only if the flow is exactly incompressible. However, in regions where the mass density does not vary much, i.e. far from interfaces, the two-phase flow will in good approximation be incompressible and this term will be small.

The isothermal approximation (10) for a two-phase (liquid and vapor) compressible flow of one component is reasonable if the thermodynamic state is little below the critical point of the substance, since latent heat $\Delta h(T)$ due to phase change tends to zero as the critical condition is approached. Therefore, for liquid–vapor systems close to the critical temperature, phase transitions lead to only small temperature changes. For this reason, although the isothermal assumption is only a first step in the development of a diffuse-interface method for the general non-isothermal case, it is not, however, without physical significance.

3. Transformation of variables

As already noted in the introduction, a numerical solution method for the governing equations of the diffuse-interface approach has to be able to cope with two additional problems compared to a numerical method for compressible single-phase flow. First, the non-monotonic Van der Waals equation of state leads to a mixed hyperbolic–elliptic system of equations in the inviscid case. Second, the highest-order spatial derivatives of mass density in the Korteweg tensor lead to dispersive behavior of the solution.

In Cockburn and Gau (1996) a study on the computation of the approximate solutions of the shock tube-like problem of one-dimensional phase-transition propagation in solids is presented. Similar as the diffuse-interface model with a Van der Waals equation of state, this problem is characterized by a non-monotonic constitutive law. Hence, in the inviscid case, the nature of the system of equations is mixed hyperbolic–elliptic. Cockburn and Gau (1996) extend the classical concept of weak solutions for purely hyperbolic systems by adding a viscous and a capillary term to the momentum equation, and by studying the limiting solutions of the new set of equations when the viscosity and the capillarity coefficient vanish while a dimensionless parameter that depends on the ratio of these two coefficients is kept constant. Stable and accurate solutions, also for nonzero values of the capillarity coefficient, have been obtained after application of a transformation of variables to the governing equations, which removes the dispersive term, caused by capillarity.

The model we present here differs in two respects from the one studied in Cockburn and Gau (1996). First, we deal with a real substance with finite macroscopic properties like viscosity and surface tension. Hence, the viscosities μ and η and the capillarity coefficient K are given non-zero functions of mass density. Second, we use an Eulerian frame of reference. We will illustrate, however, that it is still possible to apply a transformation of variables that removes the major dispersive terms from the momentum equation.

In the transformation we apply, mass density remains unchanged, whereas the new velocity vector $\hat{\mathbf{u}}$ is given by

$$\rho\mathbf{u}=\rho\hat{\mathbf{u}}-v_0(\rho)\nabla\rho, \tag{13}$$

where $v_0(\rho)$ is an arbitrary function of mass density having the dimension of kinematic viscosity. The transformed governing equations read

$$\rho_t+\nabla\cdot(\rho\hat{\mathbf{u}})=\nabla\cdot(v_0\nabla\rho) \tag{14}$$

for mass conservation, and

$$\begin{aligned}(\rho\hat{\mathbf{u}})_t+\nabla\cdot(\rho\hat{\mathbf{u}}\otimes\hat{\mathbf{u}})+\nabla p&=\nabla\cdot\left(\mu\left(\nabla\hat{\mathbf{u}}+(\nabla\hat{\mathbf{u}})^T\right)\right)\\&+\nabla((\eta-v_0\rho)\nabla\cdot\hat{\mathbf{u}})+\nabla\left(\left(\rho K-\frac{v_0}{\rho}(\eta-v_0\rho)\right)\nabla^2\rho\right)\\&-\nabla\cdot\left(\left(K+\frac{v_0^2}{\rho}+\frac{2\mu v_0'}{\rho}-\frac{2\mu v_0}{\rho^2}\right)\nabla\rho\otimes\nabla\rho\right)+\nabla\cdot(v_0(\nabla\rho)\otimes\hat{\mathbf{u}})\\&+\nabla\cdot(v_0\hat{\mathbf{u}}\otimes\nabla\rho)-\nabla(v_0\hat{\mathbf{u}}\cdot\nabla\rho)-2\nabla\cdot\left(\frac{\mu v_0}{\rho}\nabla\nabla\rho\right)\\&+\nabla\left(\left\{(-\eta+v_0\rho)\frac{v_0'}{\rho}+\frac{\eta v_0}{\rho^2}+\frac{1}{2}(K+\rho K')\right\}|\nabla\rho|^2\right),\end{aligned} \tag{15}$$

for momentum conservation. Note that the two governing equations are still in conservative form. Moreover, since the physical quantities μ,η and K are functions of mass density only, and mass density is unchanged by the transformation, these quantities still satisfy the same functional dependence.

3.1. The choice of $K(\rho)$

As in Cockburn and Gau (1996) it is possible to choose the viscosity coefficient $v_0(\rho)$ in such a way that the amount of dispersion in the transformed set of equations is kept limited. In particular, the terms in (15) with third-order derivative to the same spatial coordinate vanish if

$$v_0^2-\left(\frac{2\mu+\eta}{\rho}\right)v_0+\rho K=0. \tag{16}$$

The relevant solution of this equation is

$$v_0=\frac{2\mu+\eta}{2\rho}+\frac{1}{2}\left[\left(\frac{2\mu+\eta}{\rho}\right)^2-4\rho K\right]^{\frac{1}{2}} \tag{17}$$

provided that

$$K\leqslant\frac{1}{4\rho}\left(\frac{2\mu+\eta}{\rho}\right)^2. \tag{18}$$

In the following we will assume a specific functional dependence of $K(\rho)$ and $\mu(\rho)$, which gives rise to a particularly attractive set of transformed equations. First of all, we will follow the usual Stokes hypothesis for the second viscosity coefficient $\eta = -\frac{2}{3}\mu$. If we further assume that

$$\mu(\rho) = c_1\rho, \tag{19}$$

and

$$K(\rho) = c_2/\rho, \tag{20}$$

with c_1 and c_2 constants, the viscosity coefficient v_0 given by (17) becomes independent of mass density:

$$v_0 = \frac{2}{3}c_1 + \left(\frac{4}{9}c_1^2 - c_2\right)^{\frac{1}{2}}, \tag{21}$$

which is strictly positive, provided that $c_2 \leqslant (4/9)c_1^2$.

The possible values of the macroscopic quantity related to capillarity, namely the surface tension, are not restricted by the choice made for the coefficient K, as will be shown in Section 5. Moreover, apart from the advantage of the possibility of a transformation which removes the major dispersive term in the governing equations, this form for $K(\rho)$ has two further advantages. First, the resulting expression for the Korteweg tensor obtains its most simple form, since substitution of (20) in (4) cancels the term with $|\nabla\rho|^2$ and yields

$$\mathbf{T} = \{-p + c_2\triangle\rho\}\mathbf{I} - \frac{c_2}{\rho}\nabla\rho\otimes\nabla\rho. \tag{22}$$

Second, the term with the highest order spatial derivative in the stress tensor becomes linear in ρ. This will simplify modeling of the equation in case large-eddy simulation will be adopted as a solution method, as is envisaged for future work.

Since (16) and (20) yield

$$K + \frac{v_0^2}{\rho} - \frac{2\mu v_0}{\rho^2} = \frac{\eta v_0}{\rho^2},$$

and

$$K + \rho K_\rho = 0,$$

respectively, more terms in the transformed momentum Eq. (15) vanish: the diagonal terms in the divergence of the tensorial product $(\nabla\rho\otimes\nabla\rho)$ cancel some of the terms in the gradient of $|\nabla\rho|^2$.

In one dimension, the transformed momentum equation obtains a particularly simple form:

$$(\rho\widehat{u})_t + (\rho\widehat{u}^2)_x + [p(\rho)]_x = \left(\frac{4}{3}c_1 - v_0\right)(\rho\,\widehat{u}_x)_x + (v_0\widehat{u}\rho_x)_x, \tag{23}$$

with v_0 given by (21). Note that the factor $(\frac{4}{3}c_1 - v_0)$ in the dissipation term is always positive due to (21).

However, the range of applicability of the transformation of variables is not limited to the case of μ and K given by (19) and (20) respectively. If other expressions are taken for μ or K, the coefficient v_0 will be a function of ρ. This will lead to additional terms in the set of transformed equations.

Once the parameter v_0 has been chosen with the aid of (19) and (20), the transformed conservation Eqs. (14) and (15) with the unchanged equation of state (8) are ready to be discretized and integrated. The numerical scheme that has been used to this purpose is described in the next section.

4. The numerical method

The differential Eqs. (14) and (15) and the equation of state (8) are discretized on a Cartesian uniform grid. The spatial discretization and the time integration methods are extensions to two and three dimensions of the method by Cockburn and Gau (1996). As a first step a finite-volume method is applied for the spatial discretization. This leads to a system of ordinary differential equations, one for each variable in each grid point.

Hence, the semi-discrete scheme reads in three dimensions:

$$\frac{d}{dt}\mathbf{U}_{i,j,k} = \frac{1}{\Delta x}\left(\mathbf{F}(\mathbf{U})_{i+\frac{1}{2},j,k} - \mathbf{F}(\mathbf{U})_{i-\frac{1}{2},j,k}\right) + \frac{1}{\Delta y}\left(\mathbf{G}(\mathbf{U})_{i,j+\frac{1}{2},k} - \mathbf{G}(\mathbf{U})_{i,j-\frac{1}{2},k}\right) + \frac{1}{\Delta z}\left(\mathbf{H}(\mathbf{U})_{i,j,k+\frac{1}{2}} - \mathbf{H}(\mathbf{U})_{i,j,k-\frac{1}{2}}\right), \tag{24}$$

where $\mathbf{U}_{i,j,k}$ denotes the vector of the conserved variables ρ and $\rho\hat{\mathbf{u}}$ in grid point (i,j,k) and $\mathbf{F}(\mathbf{U})$, $\mathbf{G}(\mathbf{U})$ and $\mathbf{H}(\mathbf{U})$ denote the vectors of the fluxes in the x, y and z directions respectively. The spatial discretization method is second-order accurate and is based on central differencing: in the grid point $(i+1/2,j,k)$ an arbitrary variable u is discretized as

$$u_{i+\frac{1}{2},j,k} = \frac{1}{12}\left(-u_{i-1,j,k} + 7u_{i,j,k} + 7u_{i+1,j,k} - u_{i+2,j,k}\right),$$

and its first and second derivatives with respect to the direction x are discretized respectively as

$$\left.\frac{\partial u}{\partial x}\right|_{i+\frac{1}{2},j,k} = \frac{1}{\Delta x}\left(u_{i+1,j,k} - u_{i,j,k}\right),$$

$$\left.\frac{\partial^2 u}{\partial x^2}\right|_{i+\frac{1}{2},j,k} = \frac{1}{2(\Delta x)^2}\left(u_{i-1,j,k} - u_{i,j,k} - u_{i+1,j,k} + u_{i+2,j,k}\right).$$

In order to describe the time integration method, we denote the right-hand side of (24) by $\mathbf{A}(\mathbf{U})_{i,j,k}$. Numerical instabilities due to the non-monotonic behavior of the Van der Waals isotherm (8) near the critical point are prevented by using a three-stage, third-order accurate Total Variation Diminishing Runge–Kutta time-integration scheme (Shu and Osher, 1988), which reads

$$\mathbf{U}_{i,j,k}^{(1)} = \mathbf{U}_{i,j,k}^{(n)} + \Delta t\,\mathbf{A}(\mathbf{U}^{(n)})_{i,j,k}, \tag{25a}$$

$$\mathbf{U}_{i,j,k}^{(2)} = \frac{3}{4}\mathbf{U}_{i,j,k}^{(n)} + \frac{1}{4}\left[\mathbf{U}_{i,j,k}^{(1)} + \Delta t\,\mathbf{A}(\mathbf{U}^{(1)})_{i,j,k}\right], \tag{25b}$$

$$\mathbf{U}_{i,j,k}^{(n+1)} = \frac{1}{3}\mathbf{U}_{i,j,k}^{(n)} + \frac{2}{3}\left[\mathbf{U}_{i,j,k}^{(2)} + \Delta t\,\mathbf{A}(\mathbf{U}^{(2)})_{i,j,k}\right]. \tag{25c}$$

The solution $\mathbf{U}_{i,j,k}^{(n+1)}$ is then used to obtain the physical velocity vector $\mathbf{u}$ by means of relation (13).

The time step Δt is chosen according to the Courant–Friedrichs–Lewy **(CFL)** condition

$$\Delta t \leqslant \Gamma\Delta x\left(\frac{dp}{d\rho}\right)^{-\frac{1}{2}}, \tag{26}$$

where Γ is an empirical constant value smaller that unity, and $\left(\frac{dp}{d\rho}\right)^{-1/2}$ is the maximum value of the reciprocal of the speed of sound at the prescribed temperature. Other characteristic velocities are negligible in the test cases that we consider.

4.1. One-dimensional test simulation

In the following, we present results obtained from one-dimensional simulations with the assumptions (19) and (20). These simulations provide useful indications on the method. First, they show how the numerical solutions converge when the grid is refined. Since the equation of state is non-convex, the stability of the numerical method is not obvious when mass density assumes values that lie in the intrinsically unstable part of the solution domain. Therefore, it is important to test the method for the case of a one-dimensional two-phase system with unstable initial condition. Second, the results show the advantages of the use of the transformation of variables. To that purpose we have compared

solutions with and without transformation of variables for exactly the same problem, i.e. the same physical parameters and initial and boundary conditions and the same computational grid.

In the test case chosen the initial velocity is equal to zero, whereas the initial mass density equals 120 kg/m^3 onto which a small high wave-number perturbation is superposed. This initial value of mass density is within the unstable part of the phase diagram and any perturbation should lead to phase separation. Symmetry conditions are applied at both boundaries. Simulations have been performed on uniform grids consisting of 200, 400 and 800 points for the case with and without transformation of variables, while the time step varies with the grid spacing according to CFL condition (26). For all cases the same spatial discretization and time integration methods are applied. All simulations show a gradual initial increase of the perturbation until phase separation occurs, after which the phase boundaries move. Eventually, a steady solution is obtained, which consists of several liquid drops in a vapor background.

In Fig. 2 an enlargement of the solutions is shown at the time in which the phase separation has already occurred, but the steady state is not yet reached. Several conclusions can be drawn. First of all, both the simulations with and without transformation of variables converge to the same solution when the grid is refined. However, simulations without transformation require approximately twice as many grid points to obtain the same accuracy as simulations with transformation. In order to assess the behavior of the two methods quantitatively, in Table 1 we calculate the L_2-norm of the errors of each simulation with respect to a simulation performed on 3200 grid nodes using the transformation of variables, at the same instant of time as in Fig. 2. The errors, which are normalized with the L_2-norm of the solution on the reference grid, show that the transformation leads to the most accurate solution for any grid refinement considered here. Furthermore, they show that both methods converge quadratically in agreement with the predicted order of accuracy of the discretization scheme.

Moreover, although hard to see in the figure, the solution on the grid with 200 points contains high wave-number oscillations in the case without transformation. The method with transformation also yielded a stable, albeit rather inaccurate, solution on a grid with only 100 grid points, whereas the method without transformation turned unstable shortly after the phase separation on the same grid.

Table 1
L_2-norm of the errors of each one-dimensional simulation with respect to a reference simulation performed on 3200 grid nodes using the transformation of variables, at the same instant of time as in Fig. 2. The errors are normalized with the L_2-norm of the solution obtained on the reference grid.

Transformation	Grid points	Error
Yes	800	8.8×10^{-3}
Yes	400	3.4×10^{-3}
Yes	200	8.7×10^{-2}
No	800	1.57×10^{-2}
No	400	6.9×10^{-2}
No	200	2.8×10^{-1}

We remark that in Fig. 2, as well as in the other simulations shown next, the length of the computational domain is expressed in nondimensional units due to the scaling properties of the method described in Section 3. In particular, if the Cartesian coordinates are scaled by a reference length L, coefficients c_1 and c_2 in (19) and (20) scale as $1/L$ and $1/L^2$, respectively.

In the next section, the classical multi-dimensional test case of retraction of an initially ellipsoidal drop will be discussed, for which the grid convergence will be analyzed and results obtained with and without transformation will be compared.

5. Drop retraction

In this and in the next section, the method described above is applied to two isothermal liquid–vapor problems, widely used in the literature to test two-phase simulation methods: the so-called *drop retraction* and *two-drops collision*. For the first problem, a grid refinement study has been performed with and without application of the transformation of variables. Moreover, the steady-state result will be compared with an analytical solution.

5.1. Two-dimensional simulations

The problem of the retraction of an initially elliptical drop in its vapor is well suited to test a numerical method for simulation of two-phase flow, since in the absence of gravity and other external forces it is purely driven by interfacial forces. Equilibrium of a liquid drop that is surrounded by quiescent vapor of the same

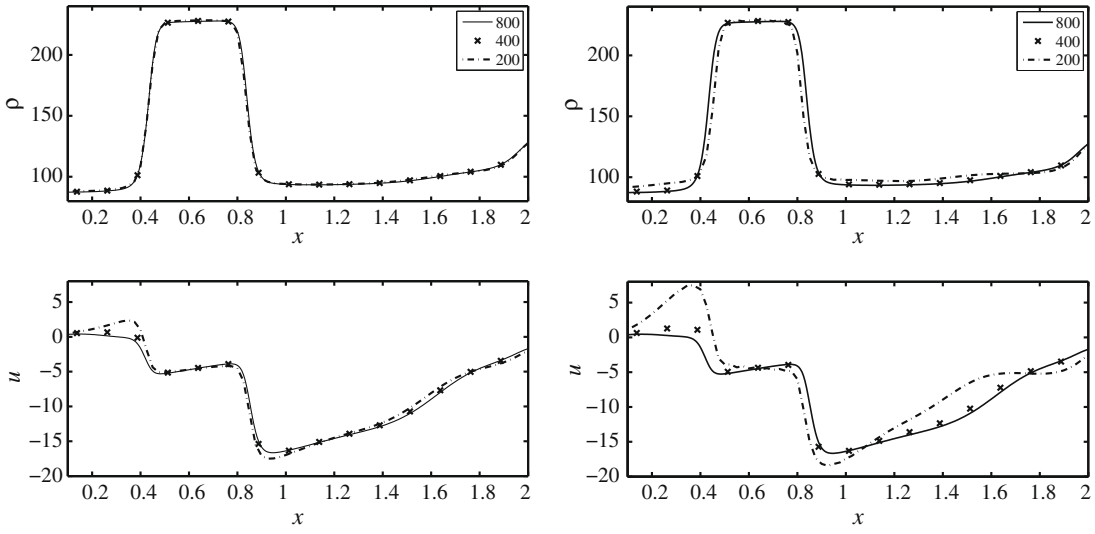

Fig. 2. Simulation of an isothermal two-phase flow of a pure substance in a one-dimensional domain, for different grid refinements, with and without application of the transformation of variables. Top: mass density. Bottom: velocity. Left: transformation of variables. Right: no transformation. Solid lines: 800, marker: 400, dash-dotted lines: 200 grid points.

substance requires the curvature of the interface to be uniform. If this is not the case, the pressure gradient and the capillary forces at the interface are unbalanced, giving rise to a nonzero velocity field in the vicinity of the interface that tends to reshape the drop into a circle. In steady state the equilibrium at the interface is described by the Laplace equation, which reads in two dimensions:

$$p_l - p_v = \frac{\sigma}{R}, \tag{27}$$

where p_l and p_v denote the pressure in the liquid and in the vapor bulk phase respectively, R is the radius of the drop and σ is the surface tension coefficient for the given substance at the prescribed temperature. In three dimensions the Laplace equation is:

$$p_l - p_v = \frac{2\sigma}{R}. \tag{28}$$

All simulations start from an initial mass density of the form:

$$\rho(x,y) = \rho_{av} - \Delta\rho \tanh\left(100\frac{(x-x_0)^2 + 2(y-y_0)^2}{x_0^2 + y_0^2} - 3\right),$$

where ρ_{av} and $\Delta\rho$ are the average and difference of the mass densities of the liquid and vapor in equilibrium at the actual temperature, and x_0 and y_0 are the coordinates of the center of the ellipse. The two bulk equilibrium values of mass density can be calculated from the isothermal Van der Waals equation of state by applying Maxwell's rule of equal areas (Aifantis and Serrin, 1983a). This initial condition corresponds to an elliptical drop in vapor, but the width of the interface is much larger than its equilibrium value. The initial velocity is set to zero. Since the solution has reflectional symmetry in both the x- and y-direction only a quarter of the domain is simulated. Symmetry boundary conditions are applied at all boundaries of the domain. Simulations are performed on a uniform Cartesian grid with 200, 400 and 800 points in the two directions and for both the cases of presence and absence of the transformation of variables (13).

Due to the difference in radius of curvature along the interface the drop will start deforming. The capillary force leads to oscillations in the shape of the drop, which are damped by the action of viscosity. After a long time a steady state is reached in which the drop has approximately a circular shape (Yue et al., 2004). Theoretically, the radius of the drop in steady state is determined by (27) and the total mass in the computational domain, which is constant because of the symmetry boundary conditions applied. Fig. 3 shows isolines of the mass density in the initial state and the final steady state.

A characteristic interfacial Reynolds number for this simulation, as proposed in Lamorgese and Mauri (2009), is defined as the ratio of capillary to viscous forces:

$$Re = \frac{\rho_{cr}^2 RTd^2}{M\mu_l^2},$$

where ρ_{cr} denotes the critical value of mass density, d the interface thickness and μ_l the dynamic viscosity of the liquid phase at equilibrium with its vapor. For the case in Fig. 3 Re is approximately 500.

In order to study grid convergence, results of the steady state mass density and pressure are presented for the case with transformation of variables in Fig. 4 on a line through the center of the drop. The figure shows the results on the three grids considered

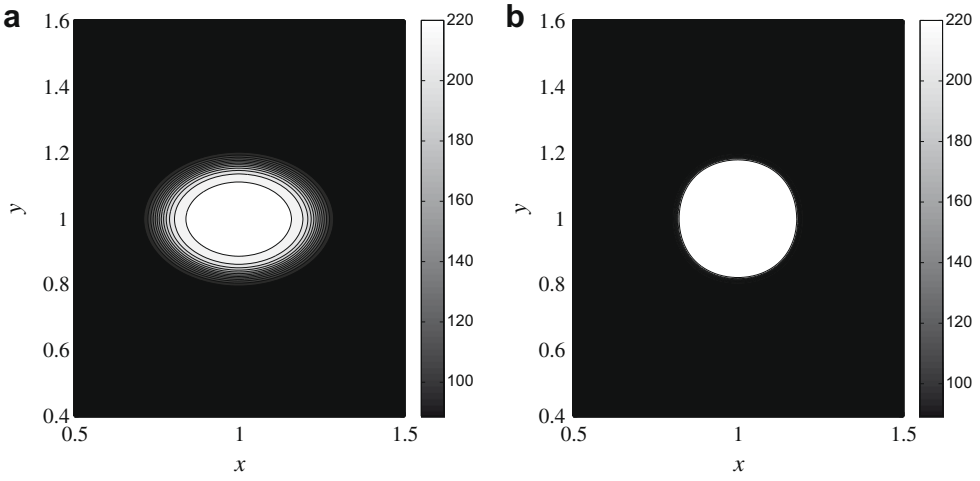

Fig. 3. Retraction of an elliptical drop surrounded by quiescent saturated vapor. (a) Initial state. (b) Steady equilibrium state. The interface is represented by means of density isolines. Length is in arbitrary units.

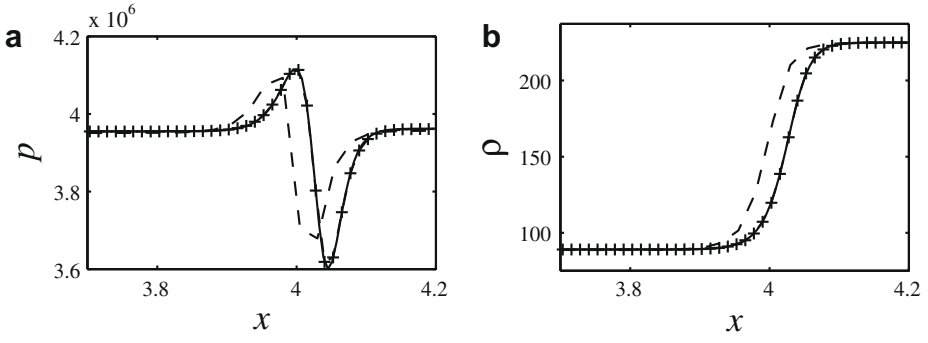

Fig. 4. Retracting drop in two dimensions. Dashed lines: 200^2, marker: 400^2, solid lines: 800^2 grid points. (a) Steady-state pressure profile. (b) Steady-state mass density profile.

here. The results on the two finest grids collapse, whereas the position of the interface between the liquid and vapor is slightly shifted on the coarsest grid. Moreover, the profiles of mass density have the same shape on all three grids. An increase in the number of grid points only leads to an increase of the number of grid points on the interface. The results of the pressure show the typical behavior caused by the Korteweg tensor. In steady state, the pressure is not constant but the sum of pressure and capillary forces is. This typical shape of the pressure is not a numerical artifact, as can be inferred from the similarity of the results on the two finest grids.

5.2. Validation

Next, a validation of the method is performed by comparing results of the simulations with analytical results. An important physical quantity in a two-phase system is surface tension, since it macroscopically represents the effect of capillarity. Therefore, an accurate calculation of this parameter is an essential requirement for any multiphase computational method. Eq. (27) or (28) can be used to obtain the value of surface tension based on the numerical solution in steady state. The following analytical expression for the surface tension holds if the width of the interface is small compared to the radius of the drop or bubble (Van der Waals, 1894):

$$\sigma = \int_{R_1}^{R_2} K(\rho)\left(\frac{d\rho}{dR}\right)^2 dR, \tag{29}$$

where R_1, R_2 are the inner and outer radii of the diffuse interface respectively and we have retained the dependence of the capillarity coefficient K on mass density. Following Cahn and Hilliard (1958) and Cahn (1959), and using expression (3) for the total free energy, we can rewrite (29) as

$$\sigma = 2\int_{\rho_1}^{\rho_2}\left[\frac{1}{2}K(\rho)\Delta f(\rho)\right]^{\frac{1}{2}} d\rho. \tag{30}$$

Here $\Delta f(\rho)$ denotes the excess Helmholtz free energy density when a unit volume of a mixture of liquid and its saturated vapor with average mass density ρ is converted into a uniform phase of the same mass density (Cahn, 1959).

Thus, the analytical calculation of surface tension is reduced to the calculation of $\Delta f(\rho)$, which can be done for given temperature and equation of state as follows. The general equation of state reads

$$T\,ds - de = pd\left(\frac{1}{\rho}\right),$$

where T is the temperature, and e and s are the specific internal energy and the specific entropy, respectively. From the definition of the Helmholtz free energy density $f = \rho(e - Ts)$, it follows at isothermal conditions that

$$d(f/\rho) = \frac{p(\rho)}{\rho^2}d\rho.$$

The Helmholtz free energy can be found by integration over mass density if the equation of state $p(\rho)$ is known. A liquid–vapor mixture at the same temperature and with homogeneous mass density equal to ρ would have the following free energy density:

$$f^{eq}(\rho) = f(\rho_v) + (\rho - \rho_v)\frac{f(\rho_l) - f(\rho_v)}{\rho_l - \rho_v}, \tag{31}$$

where ρ_l, ρ_v are the mass density of liquid and of its saturated vapor respectively. Finally, we can write $\Delta f(\rho)$ as

$$\Delta f(\rho) = f(\rho) - f^{eq}(\rho). \tag{32}$$

Table 2
Numerically obtained surface tension for various grids, for two- and three-dimensional simulations with and without transformation of variables.

Dimension	Transformation	Mesh	$\sigma \times 10^4$ (N/m)
2	Yes	200^2	7.20 ± 0.17
2	Yes	400^2	7.017 ± 0.083
2	Yes	800^2	6.965 ± 0.024
2	No	200^2	10.20 ± 0.17
2	No	400^2	7.048 ± 0.070
2	No	800^2	6.971 ± 0.017
3	Yes	200^3	6.98 ± 0.16
3	Yes	400^3	6.943 ± 0.079

Substitution of (32) in (30) leads, for our choice of temperature, capillarity coefficient and parameters in the equation of state (8), to the theoretical value of surface tension $\sigma = 6.961 \times 10^{-4}$ N/m.

This can be compared with the values obtained from the numerical results and (27), which are collected in Table 2. The shape of the interface is never exactly circular on a Cartesian mesh. The corresponding difference between maximum and minimum drop radius is used to estimate the error in the surface tension included in the table.

For the simulations which employ the transformation of variables the discrepancy between the numerical and theoretical value of surface tension ranges from 3.4% on the coarsest grid to 0.05% on the finest grid. Moreover, the decrease in the error caused by the non-circular shape of the drop reduces in agreement with the second-order accurate spatial discretization scheme employed in the method. As in the one-dimensional test case discussed in the previous section, the method without transformation requires a finer grid to work well. The numerical solution on the grid with 200 points in each direction did not converge to a steady state and the corresponding surface tension, which is based on a time average, is far from the theoretical value. On the finer grids the differences between the steady solutions of both methods are within the error estimate.

5.3. Three-dimensional simulations

For the method where the transformation of variables is applied, also three-dimensional simulations of the same test case have been performed on two Cartesian uniform meshes with 200^3 and 400^3 grid points. In order to save calculation time, the reflectional symmetry in all three directions has been used and only one eighth of the domain has been calculated. Results for the surface tension based on these simulations are included in Table 2. The accuracy of the estimation is significantly better than in two dimensions at the same grid resolution. However, the fact that

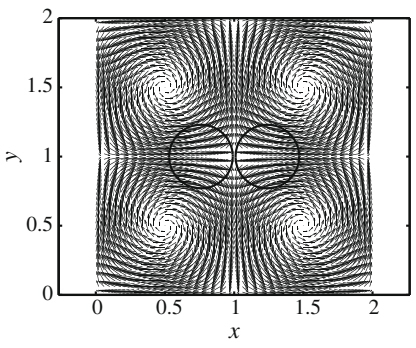

Fig. 5. Initial velocity field and droplet shape for the two-drop collision test case.

the difference between numerical and theoretical surface tension hardly decreases with increasing grid size for two grids suggests that this is a coincidence.

6. Two-drop collision

Two-dimensional, isothermal head-on collision between two identical liquid drops surrounded by vapor is a second classical benchmark simulation for multiphase simulation methods (Nobari et al., 1996). In this test case the interface undergoes topological changes, which lead to coalescence. Coalescence occurs because of attractive forces between molecules on the nearby interfaces of the two droplets. The benefit of the diffuse-interface approach over sharp-interface methods is that these forces are included in the formulation. No explicit reconnection of the interface at the moment of the closest approach of the two drops is required. In

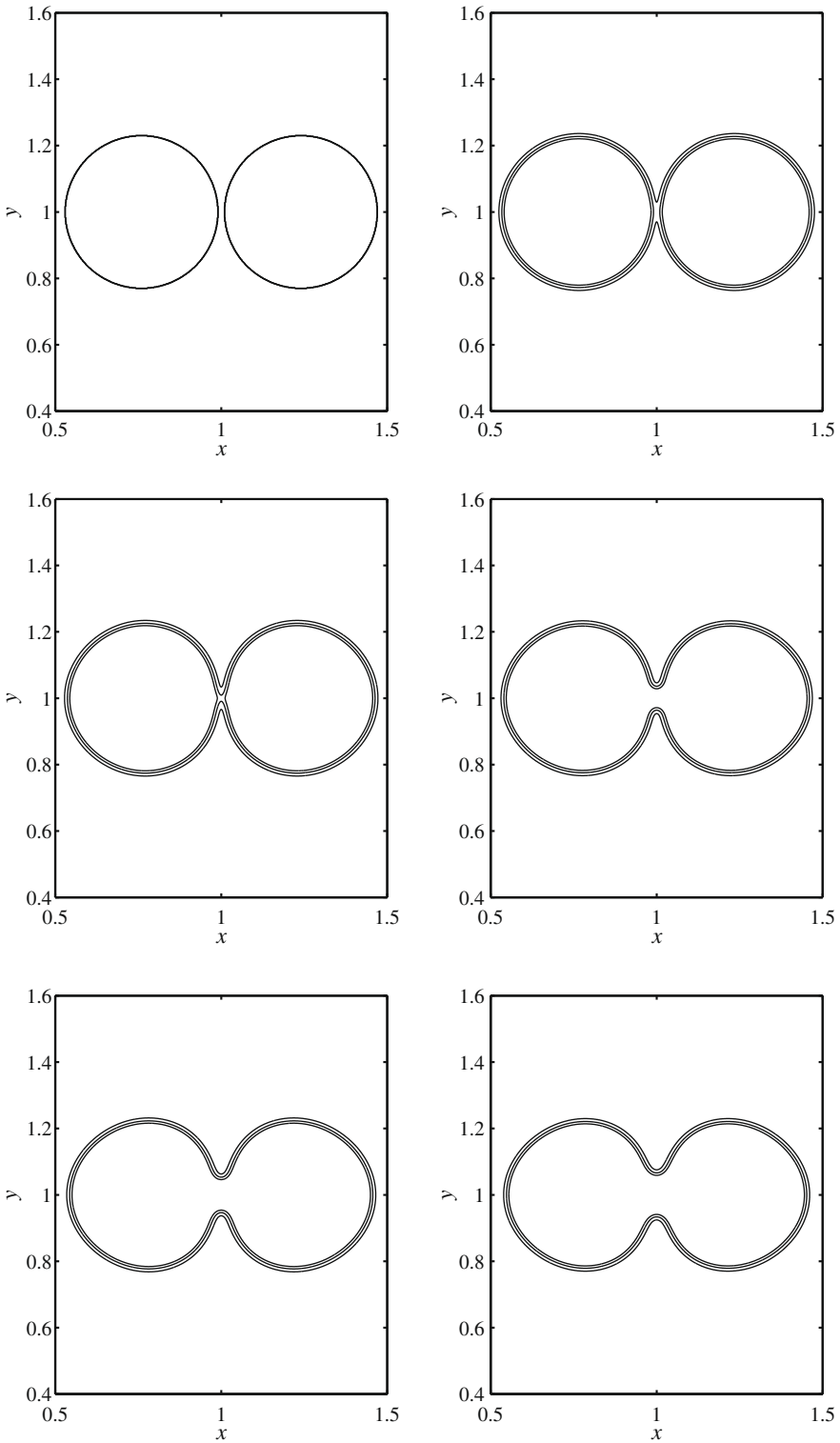

Fig. 6. Two-dimensional head-on collision between two identical liquid droplets in vapor. From left to right and top to bottom: time evolution of the simulation at equidistant times. Three isolines of mass density are shown: one at 10%, one at 50% and one at 90% of the liquid mass density in equilibrium.

the same way break-up of a drop into two smaller drops occurs automatically if the interface is constricted too far.

As a test case we consider two initially circular drops in vapor with a sharp interface in a divergence-free velocity field, which consists of four vortices in such a way that the centers of the drops initially approach each other. Due to this approaching velocity and due to the smoothing of the interface the two drops approach each other so closely that the attractive intermolecular forces lead to coalescence. The initial velocity field and the initial shape of the droplets are shown in Fig. 5.

Symmetry boundary conditions are applied on all boundaries. The initial velocity field satisfies these boundary conditions. Since the solution has reflectional symmetry in both directions, only a quarter of the domain is simulated. The computational grid is

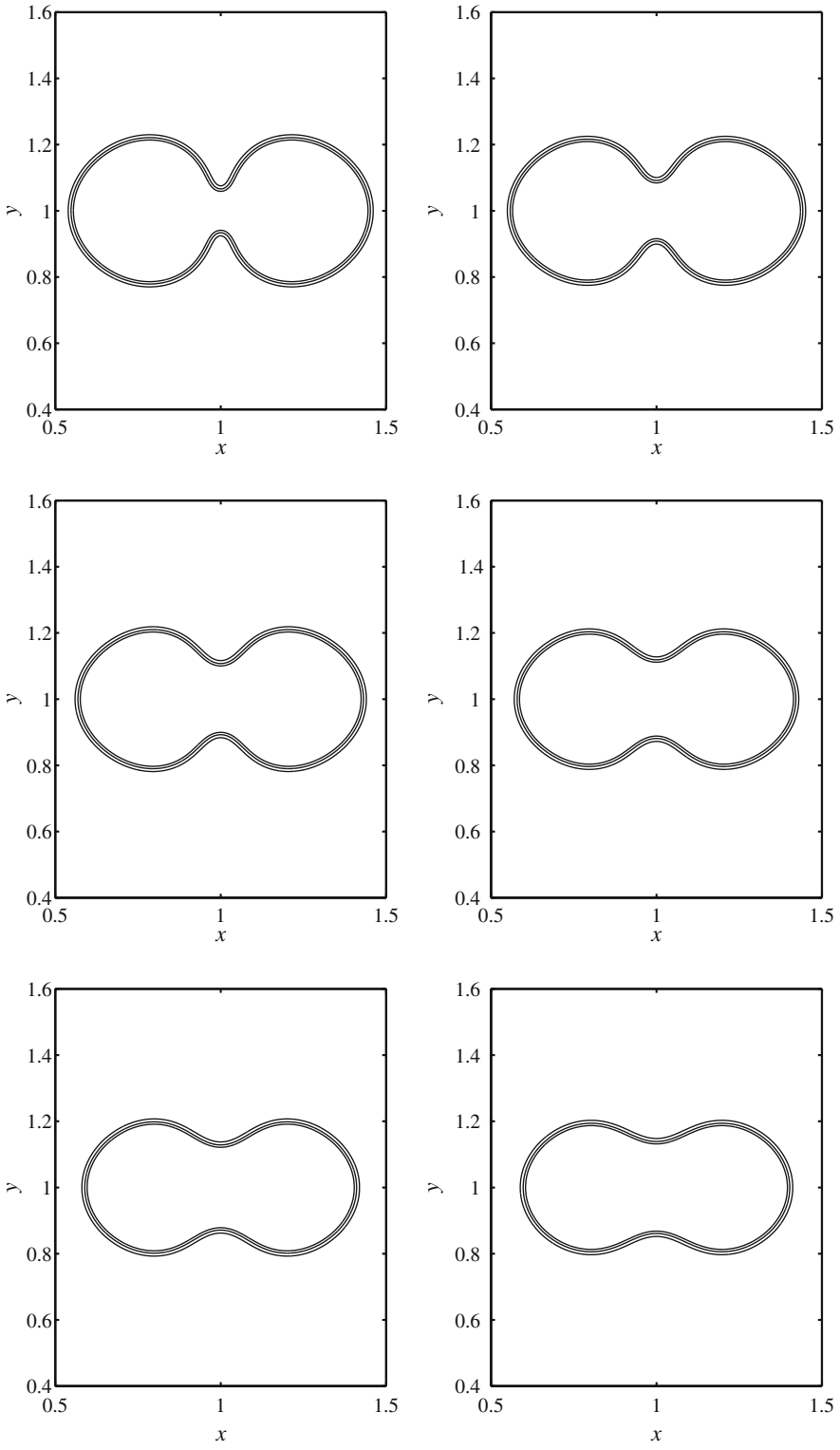

Fig. 7. Two-dimensional head-on collision of two identical liquid droplets in vapor. From left to right and top to bottom: time evolution of the simulation at equidistant times, with larger time interval than in Fig. 6. Three isolines of mass density are shown: one at 10%, one at 50% and one at 90% of the liquid mass density in equilibrium.

uniform and has 800 points in each direction. The numerical simulation is performed in the formulation with transformation of variables. Isolines of mass density are shown at several equidistant times, starting from the initial time, in Figs. 6 and 7.

After the coalescence of the drops the curvature of the interface is far from uniform and the drop keeps deforming until a state of equilibrium is reached in which the single drop is circular again. Since the problem conserves total mass, the radius of the final drop depends on the total initial mass in the domain and on the equilibrium values of mass density in the bulk liquid and vapor.

The Weber number for this type of problem, defined as

$$We = \frac{\rho V^2 D}{\sigma},$$

with ρ the drop mass density, V the magnitude of the relative impact velocity of the drops and D the drop diameter, is recognized to be the only parameter that affects the way coalescence takes place (Schotland, 1960). If the magnitude of the initial velocity field is increased, *We* is also increased and causes the drops to experience stronger deformation during coalescence. It is quite well known that the formation of so-called satellite drops is bound to occur if high-velocity jets are formed during coalescence, see for example Mansour and Lundgren (1990) and van der Geld and Vermeer (1994). In the simulation that we present in Fig. 8, the Weber number based on the maximum magnitude of the velocity field imposed at time $t = 0$ is 40 times larger than in the simulation of Figs. 6, 7, and we have removed the reflectional symmetry in both directions so that the calculation of the solution is extended to the entire domain, since now the centers of the two colliding drops are not placed in line. The first picture shows a stage of the coalescence of the two drops. The two next pictures show that in a later stage of this process the formation of satellite droplets is predicted:

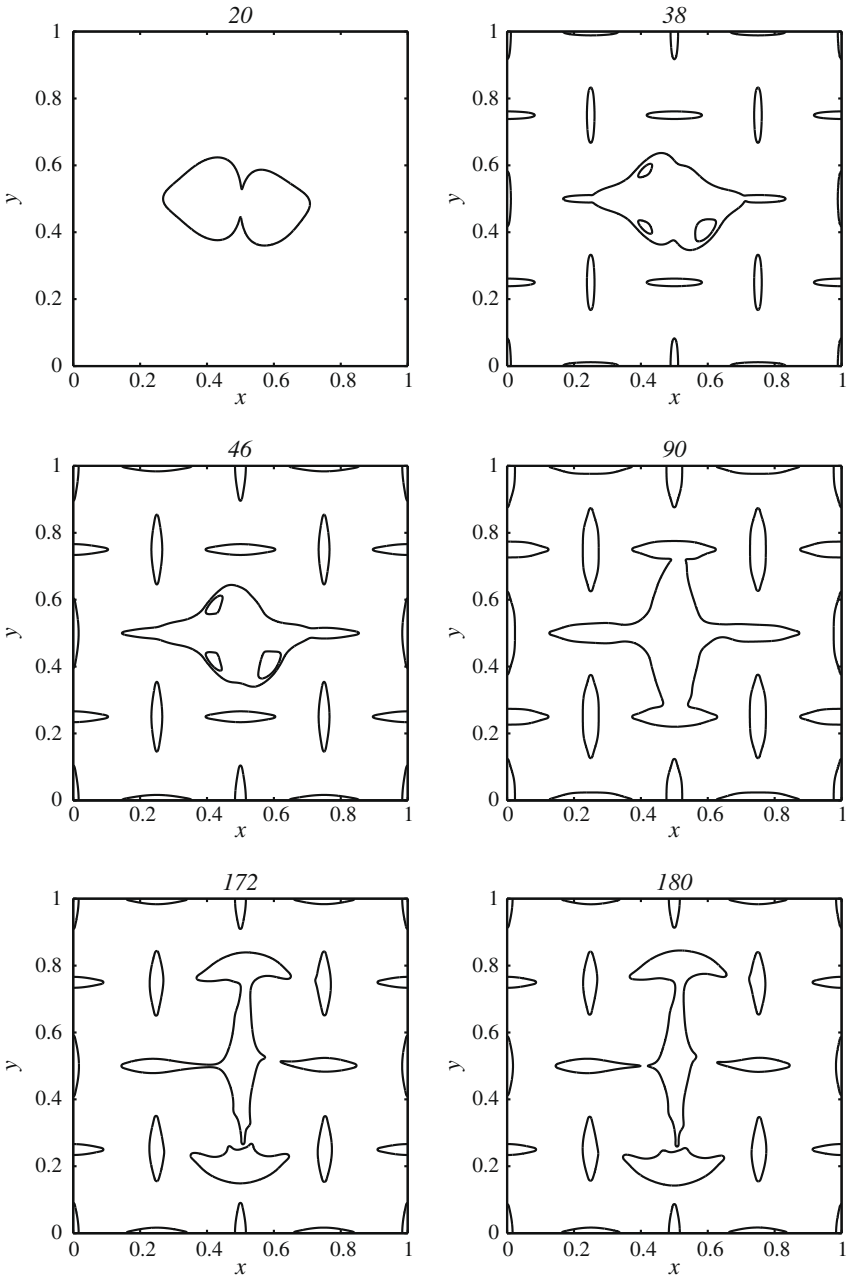

Fig. 8. Two-dimensional, asymmetric collision of two liquid droplets in vapor at high initial velocity, with symmetry boundary conditions. From left to right and top to bottom: time evolution of the simulation at arbitrary subsequent times. The isoline of mass density is shown at the average value of the liquid and vapor mass density in equilibrium.

reflection of compression waves due to boundary conditions causes local fluctuations of the mass density, from which satellite droplets originate if conditions are favorable. This is the case in the simulation considered here, as the ratio p/p_{cr} between the value of assigned pressure and the critical pressure is approximately equal to 0.95.

At this stage of the coalescence process, bubble formation inside the central drop also appears. While satellite droplets are generated by compression waves in the vapor phase, bubbles originate by effect of rarefaction waves in the liquid phase. This phenomenon is similar to the formation of cavitation bubbles, and is known to occur even at ambient pressure when a drop impinges at high velocity on a solid surface (Harlow and Shannon, 1967; Fujimoto et al., 2000). Expansion waves generated at the impact with the surface propagate, reflect and interact to produce areas of that low pressure that bubbles are formed inside the drop. In a similar manner bubbles are created in the situation described here.

The fourth picture is right after the coalescence of the central drop with satellite droplets. Finally, the two last pictures show the configuration just before and after the so-called *pinch-off* of the central drop.

7. Conclusions

The objective of the present paper was the development of a stable and accurate numerical method for isothermal two-phase flow of a pure substance near the critical point, which takes into account the finite thickness of the interface. The adoption of a diffuse-interface approach requires the incorporation of the tensor of capillary stresses. Together with a non-convex two-phase equation of state, such as the Van der Waals equation, this leads to a system of equations with dispersive and elliptic properties. A stable numerical solution method has been developed that is based on a transformation of the dependent variables and on a Total Variation Diminishing time integration technique.

The accuracy of the numerical method and its grid convergence have been assessed for the problem of the retraction of an initially non-spherical drop in vapor, both in two and in three spatial dimensions. The resulting surface tension compares well with its theoretical value. Moreover, it has been demonstrated that the transformation of variables allows the usage of coarser grids without losing accuracy. Thus, local grid refinement can be avoided at the interfacial zones if the size of the computational domain is not too large compared to the thickness of the interface.

The numerical method has also been applied to the isothermal head-on collision between two identical drops. The significance of this test case is twofold. First, unlike other two-phase models, rupture of the colliding interfacial films and subsequent coalescence of the two drops are reproduced by the numerical simulation without any need of an additional model. Second, the method proves to be able to capture the time evolution of interfaces undergoing major topological changes, such as the pinch-off of a smaller drop after the coalescence when the characteristic Weber number is sufficiently high.

It can be concluded that the numerical method described here is a useful alternative to other implementations of the diffuse-interface model for isothermal two-phase flows. In the results shown here we have chosen the dynamic viscosity to be a linear function of mass density and the gradient energy coefficient, K, to be inversely proportional to mass density. The transformation of variables can also be applied in more general conditions, but then the kinematic viscosity coefficient ν_0 will be a function of mass density and the transformed set of equations will contain additional terms. However, condition (18) limits the possibility of removing the dispersive terms from the equations for the transformed variables to moderate values of the Reynolds number based on the interface thickness.

Acknowledgements

This research is supported by the Dutch Technology Foundation STW, applied-science division of NWO (Dutch Organisation for Scientific Research), and the Technology Program of the Ministry of Economic Affairs of the Netherlands.

References

Aifantis, E.C., Serrin, J.B., 1983a. The mechanical theory of fluid interfaces and Maxwell's rule. J. Colloid Interf. Sci. 96, 517–529.
Aifantis, E.C., Serrin, J.B., 1983b. Equilibrium solutions in the mechanical theory of fluid microstructures. J. Colloid Interf. Sci. 96, 530–547.
Anderson, D.M., McFadden, G.B., Wheeler, A.A., 1998. Diffuse-interface methods in fluid mechanics. Annu. Rev. Fluid Mech. 30, 139–165.
Bongiorno, V., Scriven, L.E., Davis, H.T., 1976. Molecular theory of fluid interfaces. J. Colloid Interf. Sci. 57, 462–475.
Cahn, J.W., 1959. Free energy of a nonuniform system. II. Thermodynamic basis. J. Chem. Phys. 30, 1121–1124.
Cahn, J.W., Hilliard, J.E., 1958. Free energy of a nonuniform system. I. Interfacial free energy. J. Chem. Phys. 28, 258–267.
Chen, C.-Y., Meiburg, E., 2002. Miscible displacements in capillary tubes: influence of Korteweg stresses and divergence effects. Phys. Fluids 14, 2052–2058.
Chen, C.-Y., Meiburg, E., Wang, L., 2001. Miscible droplets in a porous medium and the effects of Korteweg stresses. Phys. Fluids 13, 2447–2456.
Cockburn, B., Gau, H., 1996. A model numerical scheme for the propagation of phase transitions in solids. SIAM J. Sci. Comput. 17, 1092–1121.
Dunn, J.E., Serrin, J.B., 1985. On the thermomechanics of interstitial working. Arch. Ration. Mech. Anal. 88, 95–133.
Fujimoto, H., Ogino, T., Takabashi, O., Takuda, H., Hatta, N., 2000. Bubble formation at impingement of a liquid droplet on a solid surface. Proc. ASME FED – 2000 253, 29–34.
Harlow, F.H., Shannon, J.P., 1967. The splash of a liquid drop. J. Appl. Phys. 38, 3855–3866.
Jamet, D., Lebaigue, O., Coutris, N., Delhaye, M., 2001. The second gradient method for the direct numerical simulation of liquid–vapor flows with phase change. J. Comput. Phys. 169, 624–651.
Korteweg, D.J., 1901. Sur la forme que prennent les équations du mouvement des fluides si l'on tient compte des forces capillaires causées par des variations de densité considérables mais continues. Arch. Néerl. Sci. Exactes Nat. Série II, Tome VI, 1–27.
Lamorgese, A.G., Mauri, R., 2009. Diffuse-interface modeling of liquid–vapor phase separation in a Van der Waals fluid. Phys. Fluids 21, 044107,1–044107,8.
Mansour, N.N., Lundgren, T.S., 1990. Satellite formation in capillary jet breakup. Phys. Fluids A 2, 1141–1144.
Mulder, W., Osher, O., Sethian, J.A., 1992. Computing interface motion in compressible gas dynamics. J. Comput. Phys. 100, 209–228.
Nobari, M.R., Jan, Y.-J., Tryggvason, G., 1996. Head-on collision of drops – a numerical investigation. Phys. Fluids 8, 29–42.
Papatzacos, P., 2000. Diffuse-interface models for two-phase flow. Phys. Scripta 61, 349–360.
Pismen, L.M., 2001. Nonlocal diffuse interface theory of thin films and the moving contact line. Phys. Rev. E 64, 021603,1–021603,9.
Schotland, R.M., 1960. Experimental results relating to the coalescence of water drops with water surfaces. Discuss. Faraday Soc. 30, 72–77.
Shu, C.-W., Osher, S., 1988. Efficient implementation of essentially non-oscillatory shock-capturing methods. J. Comput. Phys. 77, 439–471.
van der Geld, C.W.M., Vermeer, H., 1994. Prediction of drop size distributions in sprays using the maximum entropy formalism: the effect of satellite formation. Int. J. Multiphase Flow 20, 363–381.
Van der Waals, J.D., 1894. The thermodynamic theory of capillarity under the hypothesis of a continuous variation of density. Verhandel. Konink. Akad. Weten. Amsterdam (sect. 1), 1 (8), 1–56 (English translation and reprint in Rowlinson, J.S., 1979. J. Stat. Phys. 20, 200–244).
Verschueren, M., Van de Vosse, F.N., Meijer, H.E.H., 2001. Diffuse-interface modelling of thermocapillary flow instabilities in a Hele-Shaw cell. J. Fluid. Mech. 434, 153–166.
Yue, P., Feng, J.J., Liu, C., Shen, J., 2004. A diffuse-interface method for simulating two-phase flows of complex fluids. J. Fluid. Mech. 515, 293–317.